REVIEWS AND COMMENTARY ■ HOW I DO IT

Radiology

The Use and Pitfalls of Intracranial Vessel Wall Imaging:
How We Do It[1]

Arjen Lindenholz, MD
Anja G. van der Kolk, MD, PhD
Jaco J. M. Zwanenburg, PhD
Jeroen Hendrikse, MD, PhD

Online SA-CME
See www.rsna.org/education/search/ry

Learning Objectives:
After reading the article and taking the test, the reader will be able to:

- Identify the main advantages of intracranial vessel wall (VW) imaging over lumen-based methods
- Identify the basic technical requirements of intracranial VW imaging and how the imaging parameters may affect the image quality and also the constraints in image assessment
- Categorize the imaging characteristics of several intracranial vascular diseases

Intracranial vessel wall magnetic resonance (MR) imaging has gained much attention in the past decade and has become part of state-of-the-art MR imaging protocols to assist in diagnosing the cause of ischemic stroke. With intracranial vessel wall imaging, vessel wall characteristics have tentatively been described for atherosclerosis, vasculitis, dissections, Moyamoya disease, and aneurysms. With the increasing demand and subsequently increased use of intracranial vessel wall imaging in clinical practice, radiologists should be aware of the choices in imaging parameters and how they affect image quality, the clinical indications, methods of assessment, and limitations in the interpretation of these images. In this How I do It article, the authors will discuss the technical requirements and considerations for vessel wall image acquisition in general, describe their own vessel wall imaging protocol at 3 T and 7 T, show a step-by-step basic assessment of intracranial vessel wall imaging as performed at their institution–including commonly encountered artifacts and pitfalls–and summarize the commonly reported imaging characteristics of various intracranial vessel wall diseases for direct clinical applicability. Finally, future technical and clinical considerations for full implementation of intracranial vessel wall imaging in clinical practice, including the need for histologic validation and acquisition time reduction, will be discussed.

Radiology

In recent years, intracranial vessel wall (VW) magnetic resonance (MR) imaging has seen an exponential increase in popularity and clinical applicability (1,2). Several years ago, VW imaging was restricted to extracranial (peripheral) arteries, such as the carotid arteries, in which atherosclerotic "vulnerable plaques"–prone

Essentials

- The main advantages of intracranial vessel wall (VW) imaging over lumen-based methods are detection of nonstenotic lesions and further characterization of stenotic lesions that have already been detected with common angiographic methods.

- For intracranial VW imaging, a minimum magnetic field strength of 3 T is necessary to obtain a sufficient contrast-to-noise ratio (CNR) and spatial resolution to visualize the thin arterial VW and to characterize VW lesions.

- Radiologists should be acquainted with the clinical patient information and the applied imaging parameters for an optimal image assessment.

- Radiologists benefit from a systematic approach in VW assessment.

- Difficulties in assessing VW images are *(a)* variances in wall thickness not related to VW disease; *(b)* close proximity of the VW to the brain parenchyma or enhancing cavernous venous plexus; *(c)* nonpathologic contrast-enhancing areas of the VW when crossing the dura mater; and *(d)* artifacts due to motion, sensitivity encoding fold-over, free induction decay, or slow flow.

- Technical challenges include reducing acquisition time to perform both pre- and postcontrast sequences without substantial decrease in signal-to-noise ratio and CNR and histopathologic validation of VW imaging.

to causing embolism and subsequent ischemic stroke–could be assessed by using different dedicated MR imaging sequences. However, increasing evidence shows that not extracranial but intracranial atherosclerosis is the leading cause of ischemic stroke worldwide (3–6). In addition, intracranial atherosclerosis has been associated with an increased (recurrent) stroke risk and vascular dementia (4,7–9). This change of insight into causes of ischemic stroke has led to a trend toward imaging the intracranial vasculature.

Traditional imaging methods for visualizing the intracranial arteries include intra-arterial digital subtraction angiography (DSA), computed tomographic (CT) angiography, Doppler ultrasonography (US), and MR angiography. DSA can depict stenotic lesions in large, as well as small arteries, including the A2 segment of the anterior cerebral artery, M2-M3 segments of the middle cerebral artery (MCA), P2 segment of the posterior cerebral artery, and even more peripheral segments of the intracranial arteries. With unenhanced CT, arterial VW calcifications can be detected that are associated with future stroke risk (10–13). CT angiography is an easily accessible and fast procedure in patients with acute stroke and can depict stenotic lesions very accurately in the more proximal intracranial arteries and its branches (14). Doppler US can depict the VW of primarily the MCA, thereby providing (single-artery restricted) information on VW disease. Finally contrast material–enhanced and time-of-flight MR angiography, like CT angiography, can depict stenotic lesions in proximal cerebral arteries, less quickly but without additional radiation dose compared with CT angiography. However, all of these techniques, except for Doppler US, have the disadvantage of only depicting the arterial lumen (including possible stenoses) and not the culprit VW itself. Intracranial VW imaging has two major advantages over DSA, CT angiography, and MR angiography: it can depict nonstenotic lesions and it can further characterize stenotic lesions that have already been detected with common angiographic methods.

In this How I do It article, we describe the utility and practical steps for performing and interpreting intracranial VW MR images. These practical steps are based on our teaching experience of intracranial VW imaging to radiologists and neuroradiologists who have started using this method in daily clinical practice. The key questions that are often raised during their learning curve will also be addressed in this article. Key steps and common VW pathologic conditions will be shown in illustrative figures of patient examples.

The Imaging Protocol–What Do We Need?

VW Imaging Sequence Prerequisites

For intracranial VW imaging, both a high contrast-to-noise ratio (CNR) and a high spatial resolution are needed to visualize the thin arterial VW and to characterize VW lesions (1,15–19). CNR in VW imaging comprises signal contrast of the VW relative to its direct surroundings, that is, blood and cerebrospinal fluid (CSF). It is dependent on both sequence parameters and magnetic field strength, where CNR generally increases with increasing field strength. The achievable spatial resolution is also dependent on the field strength, as well as on the acquisition time. Finally, the different image contrast weightings need to be considered when developing a VW imaging protocol (1).

VW CNR.—The first step in achieving a high VW CNR is to suppress the luminal blood. Most intracranial VW imaging sequences rely on the intrinsic "black blood" properties of three-dimensional (3D) turbo spin-echo (TSE) pulse sequences, with variable flip-angle refocusing pulses (17,19–23). In these sequences, black blood is achieved by intravoxel dephasing of flowing blood, which is most effective when low-flip-angle refocusing pulses are used (17,24). Alternatively, preparation pulses can be used to obtain blood suppression, such as double inversion recovery (25), motion-sensitizing preparation pulses (26), or delay alternating with nutation for tailored excitation (DANTE) preparation pulses (20). Adding preparation pulses generally increases acquisition time. Currently, there is a need for a thorough analysis, both theoretically and experimentally, assessing the performance of the various blood suppression techniques in the presence of slow flow (directly next to the VW).

For optimal CNR, not only suppression of blood signal to depict the inner boundary of the VW, but also suppression of CSF signal to depict the outer boundary is essential, especially when outward vascular remodeling is present (27–30). At 3 T, the CNR between VW and lumen is superior to the CNR between VW and CSF on most pulse sequences. Because an inversion-recovery pulse as a CSF-suppressing technique is both time consuming and detrimental to the VW signal-to-noise ratio (SNR), these VW imaging sequences rely implicitly (without use of CSF suppression preparation pulses) or explicitly (with use of DANTE) on CSF flow for CSF suppression (19–21,31,32). Consequently, suppression of CSF will be lower in compartments where there is a slower flow of CSF, for example, around the VW and at locations where there is little CSF surrounding the vessels. However, a recent promising development for improving CSF suppression at 3 T is the incorporation of an antidriven-equilibrium pulse, which relies on T1 and T2 relaxation properties and is independent of CSF flow (32,33). At higher field strengths, such as 7 T, the higher attainable SNR enables the use of previously mentioned inversion-recovery pulse, resulting in nearly optimal CSF suppression (15).

Spatial resolution.—Due to a lack of in vivo-ex vivo correlation studies (see "Future Prospects"), it is currently not clear what minimum spatial resolution is necessary to accurately diagnose intracranial VW disease, nor is it known what spatial coverage is clinically relevant. Previous histopathologic studies have shown the intracranial arterial VW to vary in thickness from 0.2 to 0.4 mm for the distal internal carotid artery to 0.2–0.3 mm for the MCA (34). However, radiologic measurements have shown a larger VW thickness of approximately 1.0 mm for both MCA and internal carotid artery (35). Several reasons can account for this difference; for example, underestimation in histopathologic studies due to preparation techniques (cell shrinkage of 8%–20% [36,37] in histopathologic preparation) or overestimation in the radiologic studies due to partial volume effects (relatively large voxels), measurement errors, and/or pulsatility effects of the VW during acquisition. On the basis of these considerations, and given the fact that one needs at least two voxels in an object to measure its size and/or thickness accurately (38), an MR imaging sequence with 0.18-mm isotropic voxels–assuming a histologically processed wall thickness of 0.3 mm and a mean shrinkage effect of 15%–would theoretically enable highly detailed assessment of the circle of Willis and, depending on the field of view (FOV), its large and small branches (34). However, it remains to be seen whether this much detail is really necessary in clinical practice in all patient groups (39). Also, (ultra)-high-resolution sequences would be met with significant time constraints, limiting their application to cooperative patients with low morbidity or necessitating either introduction of very fast imaging techniques or compromising between spatial resolution and FOV.

To avoid these limitations, intracranial VW imaging sequences in current practice are mainly aimed at detecting larger lesions in the intracranial arteries proximal and just distal to the circle of Willis (M1, A1, P1 segments) and at the border of the M1-M2, A1-A2, and P1-P2 segments. The acquired in-plane spatial resolution of these sequences ranges between 0.4×0.4 mm^2 and 0.9×0.9 mm^2 (1,18,28,31,35,40,41). For more distal arteries, however, detection reliability will decrease because the diameter of these arteries and therefore lesions at the walls of these arteries become smaller, increasing the impact of partial volume effects (35), which needs to be taken into account when assessing the VWs in clinical practice (see "Systematic Approach of VW Assessment").

Isotropic versus anisotropic voxels.—A related question is whether and/or when to use isotropic or anisotropic voxels. Most experts in the field of VW imaging sequence development prefer sequences with isotropic voxels, which render multiplanar assessment more feasible. Compared with, for example, the carotid artery, intracranial arteries are often tortuous and have varying orientations, making multiplanar reconstruction an important asset in assessment of these arteries. In anisotropic sequences, a very high in-plane spatial resolution can be achieved within reasonable acquisition times, enabling detailed assessment of VW lesions and atherosclerotic plaque characterization when the FOV is placed perpendicular to the lesion. However, due to the larger through-plane voxel size, small lesions are subject to partial volume effects. Therefore, it may well be dependent on the specific clinical question on a single-patient basis which type of sequence (isotropic versus anisotropic voxels) to use. For instance, a radiologist may consider isotropic sequences in patients with no previous imaging or known VW lesion as a method of screening the intracranial arteries, while an anisotropic sequence could be used to assess a known lesion.

The advantage of interpreting VW images in multiple planes is currently not supported by much research data. The results of recent studies suggest that the use of transverse images alone may be

sufficient for the interpretation of VW images (42,43). In one of these studies, 3D sequences with a high in-plane spatial resolution and a larger section thickness were either performed in the transverse plane or perpendicular to the MCA. VW lesions of the MCA were also detected on the images that were acquired nonperpendicular to the artery.

Two-dimensional versus 3D imaging.—To increase in-plane spatial resolution, two-dimensional (2D) spin-echo sequences can be used as an alternative to 3D methods (1,28,31,44). The 2D in-plane spatial resolution is equivalent to that of 3D, and volume-averaging errors due to thicker sections (2 mm, no gap) are alleviated by repeating the sequences in sagittal and/or axial planes targeted to a lesion in question. Sequence acquisition times are short (approximately 3 minutes) with good SNR. The drawbacks of these 2D spin-echo methods are the need to target a specific lesion due to limited coverage to keep imaging times short and the increased dependence on correct positioning of the FOV. Two-dimensional methods can therefore best be applied in cases in which there is a known intracranial stenosis on which the FOV can be focused and has highest value in characterizing the underlying pathologic process (eg, atherosclerotic plaque characterization).

Field strength.—A further consideration is what field strength to use. In our experience and that of others (2), 1.5 T does not achieve sufficient SNR and CNR within a reasonable acquisition time. Therefore, a field strength of 3 T or higher is mandatory. In light of the increased availability of 3-T MR imaging platforms, this makes intracranial VW imaging feasible in many hospitals worldwide. The advantage of a 7-T field strength is an increased SNR and CNR compared with 3 T, which enables better intrinsic image contrast and a higher spatial resolution within a reasonable acquisition time (16,18). Specifically for VW imaging, the higher SNR also enables the use of the inversion-recovery pulse mentioned above to completely suppress the CSF and a large FOV for whole-brain coverage; however, this

does come at the cost of a lower spatial resolution to keep acquisition times within limits. Nonetheless, although current 7-T VW imaging pulse sequences have a lower or comparable spatial resolution compared with published (and our own) 3-T sequences, visualization of the VW was still found superior at 7 T, mainly due to higher CNR and more optimal CSF suppression (45). However, only approximately 60 7-T MR imaging platforms exist worldwide. Also, the inhomogeneous B_0 and B_1 fields can still hamper assessment of peripheral parts of the brain, such as in the Sylvian fissure, although this is improving over time due to the continuous development of the technology. Combined with the fact that 7-T MR imaging has not yet been officially approved for clinical diagnostic imaging, 7-T VW imaging sequences are mainly used for research purposes and specific challenging clinical cases (eg, cerebral vasculitis).

Image contrast weighting.—Mirroring pulse sequence development in the extracranial carotid artery, pulse sequences with different image contrast weighting (eg, T1-, T2-, and proton density weighted) have also been developed for assessing the intracranial VW. Theoretically, the ideal VW imaging protocol would include images of all three image contrast weightings and a T1-weighted sequence after contrast agent administration to assess intracranial VW disease in the same fashion as has been done for years for their extracranial counterparts (46). However, no clear evidence yet exists on the clinical relevance of multicontrast MR imaging protocols for intracranial VW disease. With the relatively long acquisition times of these VW sequences, most of the currently used intracranial VW imaging protocols rely on T1-weighted imaging, because of its benefits in the detectability of contrast enhancement after contrast agent administration and favorable imaging characteristics when distinguishing the VW from its surrounding tissue and (if present) plaque components (47).

Our 3-T Protocol

The 3-T MR imaging systems at our center (Achieva 3.0T; Philips Healthcare,

Best, the Netherlands) were recently equipped with a 32-channel phased-array sensitivity encoding head coil. Previously, we used an eight-channel head coil. We clinically use a 3D T1-weighted volumetric isotropically reconstructed TSE acquisition, or VIRTA, sequence (adapted from Qiao et al) (17,42) that is performed after contrast material administration only (gadobutrol, Gadovist 1.0 mmol/mL, single dose, adjusted to patient weight; Bayer Schering Pharma, Newbury, England). The images are acquired at an anisotropic spatial resolution of $0.5 \times 0.5 \times 1.0$ mm^3 that is subsequently reconstructed to $0.5 \times 0.5 \times 0.5$ mm^3 isotropic resolution. We have chosen this particular spatial resolution, which is considerably below the "ideal" spatial resolution of $0.18 \times 0.18 \times 0.18$ mm^3 mentioned above, because of the limitations regarding acquisition time and SNR. Also, in a recent small study, we found that sequences with a lower spatial resolution (0.5 mm $\times$ 0.5 mm $\times$ 1.0 mm) and a short imaging duration (4 minutes 39 seconds) have a good subjective quality score and good performance with respect to lesion detection (39). An anisotropic sequence was chosen for two main reasons: *(a)* In our experience, assessment of the in-plane sections, planned in a transverse oblique plane to image the circle of Willis in the classic anatomic way (Fig 1), most often will suffice for detection of larger lesions and *(b)* we mainly use this sequence to detect VW enhancement, which is less dependent on partial volume effects. In this regard, an anisotropic voxel size can in our opinion be a good compromise with an increase in SNR and shorter acquisition times. However, the above-mentioned drawbacks of anisotropic sequences always need to be taken into account when assessing the images.

In the VIRTA sequence, black blood is obtained by means of low-flip-angle refocusing pulses. To optimize CSF suppression, we use the antidriven-equilibrium method (17,33,39). Because CSF suppression is not optimal with use of this method, we have currently started implementing DANTE for better CSF suppression. Because the FOV of the sequence is
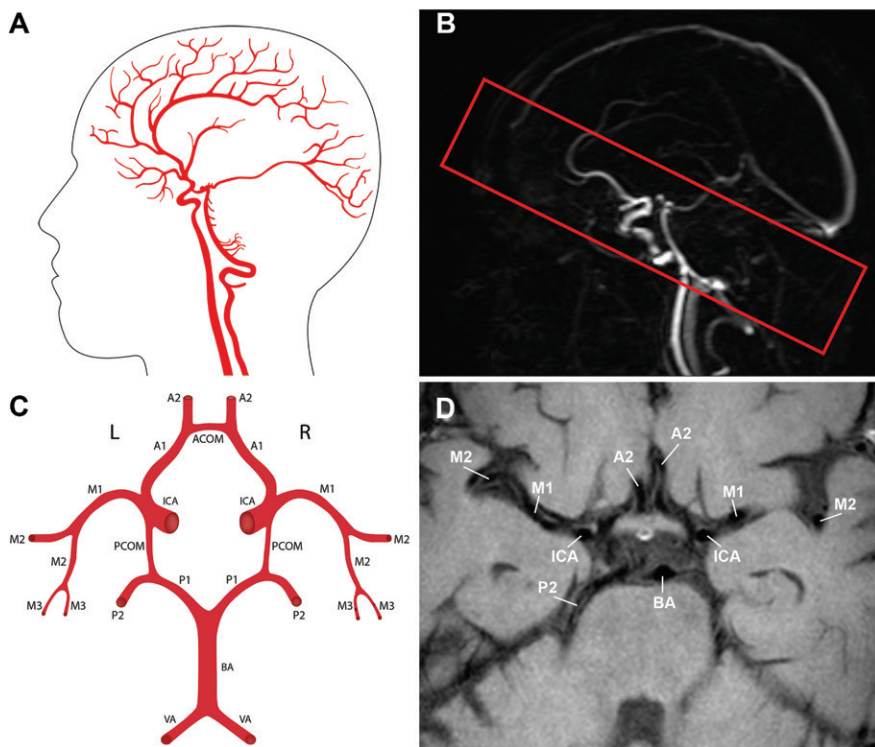
Figure 1

Figure 1: *A,* Sagittal view of the anterior circulation intracranial arteries and, *B,* corresponding phase-contrast angiographic image used in our clinic for planning the FOV (45-mm feet-head, red box) in a transverse oblique plane to include all large intracranial arteries of the anterior circulation. *C,* Transverse view of the large intracranial arteries of the circle of Willis and, *D,* corresponding transverse oblique 3-T T1-weighted intracranial VW MR image, in which most anterior circulation arteries can be seen in one section. *A1* and *A2* = segments of the anterior cerebral artery; *ACOM* = anterior communicating artery; *BA* = basilar artery; *ICA* = internal carotid artery; *M1, M2,* and *M3* = segments of the MCA; *P1* and *P2* = segments of the posterior cerebral artery; *PCOM* = posterior communicating artery; *VA* = vertebral artery.

restricted in the through-plane direction–measuring 45 mm thickness–care must be taken to plan the FOV correctly (Fig 1). Key parameters of our 3-T protocol are shown in Table 1.

Our 7-T Protocol

The 7-T MR imaging platform at our institution (Philips Healthcare, Cleveland, Ohio) is equipped with a 32-channel receive coil and a volume transmit/receive coil for transmission (Nova Medical, Wilmington, Mass). We use a T1-weighted magnetization-prepared inversion-recovery TSE intracranial VW sequence (15,48) performed before and after contrast material administration, with acquired isotropic resolution of $0.8 \times 0.8 \times 0.8$ mm^3

that is reconstructed to $0.49 \times 0.49 \times 0.49$ mm^3 isotropic resolution. The pulse sequence includes an inversion recovery pulse that results in nearly complete CSF suppression and uses low and varying refocusing pulse angles for obtaining black blood. The FOV encompasses the entire brain (190 mm), which, in combination with the isotropic spatial resolution, does not require additional planning in oblique angles. B$_0$ shimming and dielectric pads are additionally used to decrease inhomogeneity of the main magnetic and radiofrequency transmit field, which otherwise can result in considerable signal loss in both temporal lobes (including the M2-M3 trajectory) (49). Key parameters of our 7-T protocol are shown in Table 2.

Use of Contrast Agents

The use of contrast material–enhanced MR imaging is considered a necessary component of VW imaging protocols (1,2). Sensitivity for contrast enhancement depends on optimal timing of contrast agent injection. Currently, no head-to-head comparisons between VW imaging sequences at different time points after contrast agent injection have been performed. For timing of contrast enhancement at standard brain MR imaging sequences, results from studies in brain tumors are generally used (50). As a general rule, optimal timing of sequence acquisition is between approximately 5–10 minutes after contrast agent injection; contrast enhancement may be weak within the first 5 minutes after injection, and evidence of the added value of a late phase acquisition (> 10 minutes) is lacking. Because many of the current VW imaging sequences have an acquisition duration of between 5 and 7 minutes, the ideal start time would be 5 minutes after contrast agent injection. At our institution, we either perform one anatomic sequence after contrast agent injection–such as an axial T2-weighted TSE or diffusion-weighted imaging sequence–or implement a 5-minute break before starting the VW imaging sequence.

The choice of whether or not to obtain both pre- and postcontrast images depends on both the specific setting and clinical question. At 7 T, we perform the VW imaging sequence before and after contrast material administration, because we mainly examine patients in a research setting or challenging cases and therefore have time (45–60-minute time slot) to acquire both pre- and postcontrast images in addition to the standard anatomic brain images. With this setup, contrast-enhancing lesions can be distinguished from nonenhancing lesions with a high signal intensity by comparing pre- and postcontrast images. However, within the context of fixed, shorter MR imaging time slots and a maximum acquisition time based on patient comfort, in clinical practice, it is often necessary to limit the time for intracranial VW imaging at 3 T. An option that reduces total protocol time, and which we currently use at our

Table 1

3-T VW Imaging Protocol Used at Our Institution

Imaging Parameter	Diffusion-weighted Imaging	3D TOF MR Angiography	2D T2 FLAIR	3D T1 VIRTA with Contrast Agent	3D T1 TFE with Contrast Agent
FOV (mm^3)	230 × 230 × 140	200 × 200 × 70	230 × 183 × 140	200 × 167 × 45	230 × 230 × 160
Acquisition orientation	Transverse	Transverse	Transverse	Transverse oblique	Transverse
Acquisition spatial resolution (mm^3)	0.96 × 1.22 × 4.0	0.4 × 0.7 × 1.0	0.65 × 0.85 × 4.0	0.5 × 0.5 × 1.0	1.0 × 1.0 × 1.0
Reconstructed spatial resolution (mm^3)	0.45 × 0.45 × 4.0	0.36 × 0.36 × 0.5	0.41 × 0.41 × 4.0	0.5 × 0.5 × 0.5	0.96 × 0.96 × 1.0
TR/TE/TI (msec)	4056/68/-	22/3.5/-	10000/120/2800	1500/32/-	8.5/3.9/1016
Flip angle (degrees)	90	18	120	90	8
Echo spacing (msec)	…	…	9.6	4.5	…
MPIR TSE factor	…	…	24	56 + 4	…
Oversampling factor	…	…	…	1.8	1.4
Readout bandwidth (Hz)	15.1	522.7	218.1	643.4	189.8
No. of signals acquired	2	1	1	1	1
Sensitivity encoding factor	3 (AP)	2 (RL)	2 (RL)	1.5 (RL)	3 (RL)
Acquisition time	1 min 25 sec	5 min 12 sec	5 min 0 sec	8 min 3 sec	2 min 29 sec

Note.—AP = anteroposterior direction, DW = diffusion weighted, FLAIR = fluid-attenuated inversion recovery, MPIR = magnetization-prepared inversion-recovery TSE (48), RL = right-left direction, TE = echo time, TI = inversion time, TR = repetition time, TFE = turbo field echo, VIRTA = volumetric isotropically reconstructed TSE acquisition (43).

Table 2

7-T VW imaging Protocol Used at Our Institution

Imaging Parameter	3D T1 MPIR TSE	DW Imaging	3D T1 MPIR TSE with Contrast Agent	Inflow SWI with Contrast Agent (3 TEs)	3D T2 FLAIR with Contrast Agent
FOV (mm^3)	250 × 250 × 190	220 × 220 × 123	250 × 250 × 190	190 × 190 × 102	250 × 250 × 190
Acquisition orientation	Sagittal	Transverse	Sagittal	Transverse	Sagittal
Acquisition spatial resolution (mm^3)	0.8 × 0.8 × 0.8	1.5 × 1.5 × 1.5	0.8 × 0.8 × 0.8	0.4 × 0.5 × 0.6	0.8 × 0.8 × 0.4
Reconstructed spatial resolution (mm^3)	0.49 × 0.49 × 0.49	1.5 × 1.5 × 1.5	0.49 × 0.49 × 0.49	0.4 × 0.4 × 0.3	0.49 × 0.49 × 0.49
TR/TE/TI (msec)	3952/37/1375	17659/57-	3952/37/1375	21/2.3*/-	8000/300/2200
Flip angle (degrees)	120	120	120	30	90
Echo spacing (msec)	3.3	…	3.3	…	4.7
TSE factor	169 (including 10 start-ups)	…	169 (including 10 start-ups)	…	125 (including 1 start-up)
Oversampling factor	1	…	1	v	1
Readout bandwidth (Hz)	934.8	23.6	934.8	557.0	410.9
No. of signals acquired	2	1	2	1	1
Sensitivity encoding factor	2 (AP) and 3 (RL)	2.5 (AP)	2 (AP) and 3 (RL)	2.5 (RL)	2.5 (AP) and 3 (RL)
Acquisition time	10 min 40 sec	6 min 10 sec	10 min 40 sec	9 min 18 sec	10 min 48 sec
Head coil	32 channel	32 channel	32 channel	32 channel	32 channel

Note.—AP = anteroposterior direction, DW = diffusion weighted, MPIR = magnetization-prepared inversion-recovery TSE (48), RL = right-left direction, SWI = susceptibility-weighted imaging, TE = echo time, TI = inversion time, TR = repetition time, VIRTA = volumetric isotropically reconstructed TSE acquisition (43).
* Delta TE = 7.2 msec for second and third echo time.

institution, is to only acquire postcontrast images. In our experience, most VW lesions–even when not enhancing–can be detected on the postcontrast VW imaging sequence and it saves half the acquisition time relative to the combination of a pre- and postcontrast sequence. Still, studies are needed to compare this alternative approach (postcontrast only) with the classic approach (pre- and postcontrast). One of the major limitations of using a postcontrast VW imaging sequence only is that findings such as intraplaque hemorrhage and intracranial arterial dissections may be missed (51).

Other Necessary Sequences
Other, more "conventional" MR imaging sequences also add helpful information when used in combination
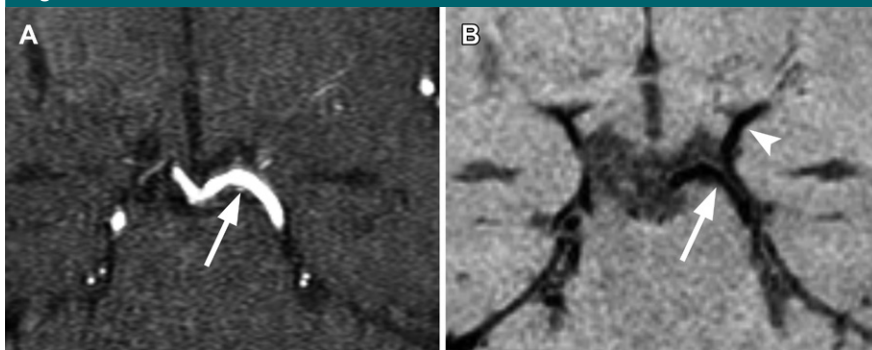
Figure 2

Figure 2: *A,* 3-T transverse TOF MR image (voxel size, 0.4 × 0.7 × 1.0 mm³) and, *B,* corresponding 3T transverse oblique precontrast T1-weighted VW image (voxel size, 0.5 × 0.5 × 1.0 mm³), both zoomed in on the left P1/P2 bifurcation of the posterior cerebral artery (arrow). On the VW image *(B)*, the basal vein of Rosenthal can be seen coursing directly lateral to the PCA (arrowhead), which is not visible on the TOF MR image *(A)*.
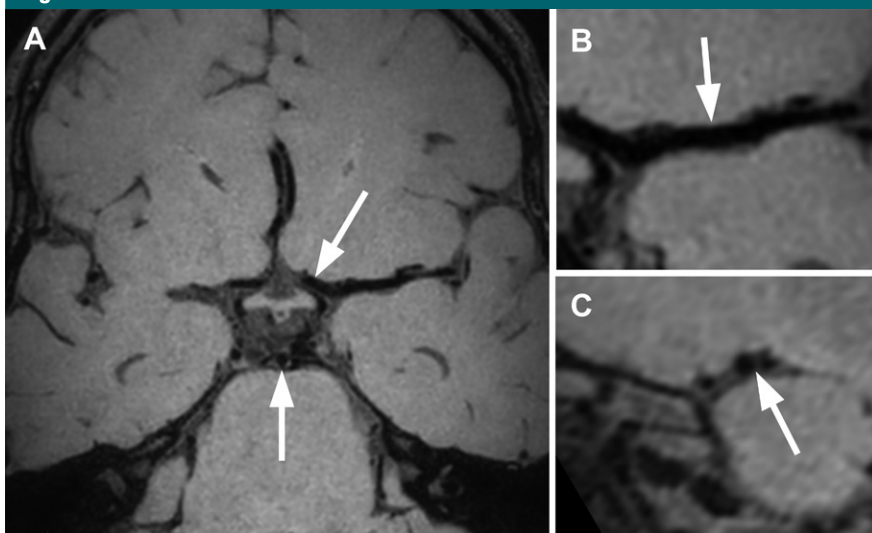
Figure 3

Figure 3: *A,* 3-T oblique (transverse/coronal) precontrast T1-weighted VW image (voxel size, 0.5 × 0.5 × 1.0 mm³) in a 29-year-old healthy volunteer. In this single section, most large intracranial arteries of the circle of Willis are (partially) visible, for example, the left A1 segment of the anterior cerebral artery and basilar artery (arrows). *B,* Zoomed image of the M1 segment of the left MCA. The VW (arrow) can barely be seen because of its close proximity to the brain parenchyma, which has comparable signal intensity. *C,* Reconstructed sagittal image (0.6 × 1.0 in-plane spatial resolution) of the left MCA (arrow). The quality and detail are marginally lower compared with the transverse oblique image because of the anisotropic voxel size.

with intracranial VW imaging. MR angiographic methods, such as contrast-enhanced MR angiography or time-of-flight (TOF) MR angiography, are particularly helpful to assess the arterial lumen and to identify the specific arteries to which the visualized VWs belong (Fig 2). Also, in case of a small FOV, these techniques can guide FOV planning centered on the circle of Willis or focused on a specific (stenotic) VW lesion. Contrast-enhanced MR angiography during first contrast agent passage clearly shows the arterial vasculature and is less sensitive to slow-flow artifacts compared with TOF MR angiography. Furthermore, with strong elongation of the arterial vasculature it is also less sensitive to a signal decrease of cranial-caudal flow, for

example, in a strongly elongated MCA. Nonetheless, TOF MR angiography is still a sensitive method to detect stenotic lesions and is the workhorse in most centers for the detection of vascular disease, including aneurysms of the intracranial vasculature (52). Because it is not dependent on first contrast agent passage, acquisition time can be invested to increase the spatial resolution.

Other pulse sequences that can be of additional value in VW imaging assessment depend on the specific clinical question and include *(a)* T2-weighted TSE sequence that can confirm the absence of a flow void in the arterial lumen in a patient with an arterial occlusion, *(b)* T1-weighted anatomic sequence for both assessment of normal anatomy and for use as precontrast sequence for (mainly tissue) enhancement, *(c)* T1-weighted fat-suppressed sequence that can depict a subintimal hematoma in patients with an arterial dissection that involves both the extracranial and intracranial segments, and *(d)* fluid-attenuated inversion recovery and diffusion-weighted imaging sequence for localizing white matter lesions and old and recent ischemia possibly associated with VW disease. The full VW imaging protocol used at our institution, including key pulse sequence parameters, can be found in Tables 1 and 2.

Patient Preparation

Proper patient preparation plays an important role in the acquisition of high-quality intracranial VW images. The patient (or legal representative) needs to be informed about the MR imaging examination, and the MR imaging staff needs to assess if any possible contraindications for MR imaging (claustrophobia, contraindicated metal objects in or on the body, pregnancy) or for gadolinium-containing contrast agents (known allergic reaction to gadolinium-containing contrast agent, severely impaired renal function) exist. Also, because of the relatively long acquisition time of VW imaging sequences, imaging staff needs to assess whether the patient is clinically able to undergo
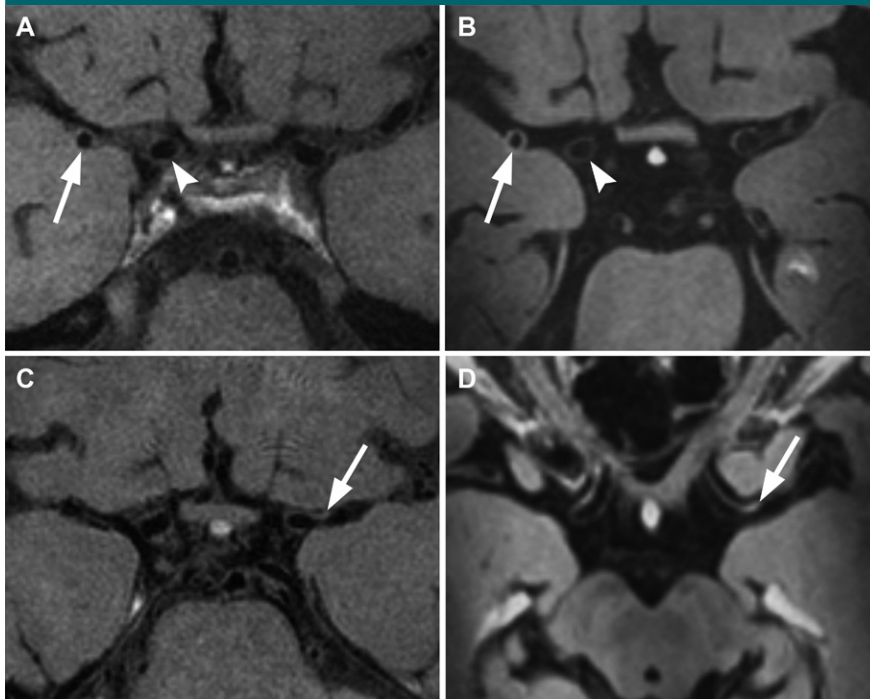
Figure 4

Figure 4: *A, B,* Images in a 68-year-old woman with a recent right-sided ischemic stroke, successfully treated with thrombolytic therapy. Concentric enhancing VW thickening is seen in the right MCA (arrow) compared with the normal appearing distal ICA (arrowhead) on 3-T T1-weighted *(A)* and 7-T T1-weighted magnetization-prepared inversion-recovery TSE *(B)* postcontrast VW images. *C, D,* Images in a 72-year-old woman with a recent transient ischemic attack. Postcontrast 3-T *(C)* and 7-T *(D)* VW images show an eccentric VW lesion (arrow) in the left MCA (just distal to the intracranial internal carotid artery bifurcation).

the examination: It may be challenging to lay still for a long period of time, especially for neurologically impaired patients. Prior to imaging, a peripheral intravenous catheter is placed in the antecubital vein for contrast agent administration (42,43,53).

Our complete VW imaging protocol (Tables 1, 2) takes approximately 23 and 48 minutes for the 3-T and 7-T protocol, respectively. The VW imaging sequence has an acquisition time of 8 minutes 3 seconds for the 3-T and 10 minutes 40 seconds for the 7-T protocol. VW imaging sequences are susceptible to motion artifacts because of the relatively long acquisition duration, and visibility of the VW decreases rapidly when patients move their head during acquisition. We therefore use foam cushions positioned around the patient's head to aid in limiting movement artifacts.

Pre-assessment Case Preparation– What Do We Need to Know?

Clinical Information

For a complete assessment of intracranial VW images, several clinical aspects are important to know. In general, when requesting VW imaging the actual clinical status of the patient (neurologic status, ability to lie still for a prolonged period of time) should be reported to assess the a priori chance of acquiring images of sufficient diagnostic quality. Next, a specific clinical question is important for defining a patient-tailored VW imaging protocol. For instance, if the clinician is suspicious of disease in the anterior cerebral vasculature, the (small) FOV of the 3-T sequence needs to be placed in a more transverse orientation in line with the arteries of the anterior circulation part of the circle of

Willis. When the area of interest lies predominantly in the posterior circulation, a more transverse oblique angulation can be used to include a longer trajectory of the basilar and vertebral arteries. On the other hand, when there is suspicion of a dissection or intraplaque hemorrhage, a precontrast VW imaging sequence can be added to a postcontrast-only protocol. Further, previous (MR imaging) examinations showing arterial disease (eg, stenoses) at conventional sequences need to be taken into account for both FOV planning and evaluation of progression.

The patient's treatment status is another important clinical feature for VW imaging assessment. For instance, when a patient with cerebral vasculitis is treated with prednisolone, it is important to know when treatment has commenced relative to the time of the imaging examination: VW enhancement may be lower or have disappeared altogether. Also, in case of an ischemic infarct that has been treated with thrombolysis or intra-arterial treatment, there may be local VW enhancement present at the location of the previous occlusion (54,55). Finally, if a patient has undergone an MR imaging examination that included contrast agent administration less than 12 hours before VW imaging, there may be residual contrast enhancement on the subsequent precontrast VW images.

Common Indications

At our institution, the most common indication for our 3-T VW imaging protocol is a suspected cerebral vasculitis (either primary angiitis of the central nervous system or due to other causes). When this suspicion is raised by the clinician, a spectrum of symptoms is often present that can also indicate the presence of other vascular diseases, such as small vessel disease or large artery atherosclerosis with unstable plaques. VW imaging can assist in differentiating between these vascular diseases but may also be helpful during follow-up and evaluation of the received treatment. Other vascular diseases in which VW imaging may be indicated are the detection or evaluation (evolution) of large artery

Table 3

Commonly Seen Imaging Characteristics for Different Intracranial VW Diseases

VW Disease	Stenosis at MR Angiography/CT Angiography	VW Thickening	Location	Enhancement*	Special Considerations	Image Example
Intracranial atherosclerosis (35,42,47,56,70,72)	Equally present and not present	Eccentric	More widespread, distal ICA/vertebral, focal lesions	Equally present and not present	Plaque characterization, intraplaque hemorrhage†	Figure 4
CNS vasculitis (73,74)	Often present	Concentric	More widespread, long trajectory	Virtually always present	Effect of steroid therapy Guiding best location for biopsy	Figure 9
Moyamoya disease (75–79)	Equally present and not present	Concentric	Distal ICA, proximal MCA	Equally present and not present	…	Figure 10
Arterial dissection (80–83)	Virtually always present	Eccentric	Distal ICA/vertebral	Often present	Detection of hematoma and flap, added value of fat suppression in case of an extracranial dissection	Figure 11
Intracranial aneurysm (69,84–87)	Equally present and not present		…	…	Often enhances when symptomatic, difficult to assess when SAH is present	Figure 12
RCVS (73,74,88)	Often present	Concentric	More widespread	Often not present	String-of-beads on angiograms	…
Iatrogenic (after thrombectomy) (54,55)	Equally present and not present	Eccentric/concentric	Thrombectomy site	Often present	…	Figure 8

Note.—CNS = central nervous system, ICA = internal carotid artery, RCVS = reversible cerebral vasoconstriction syndrome, SAH = subarachnoid hemorrhage.

* Concordant with contrast enhancement of extravascular disease, contrast enhancement of intracranial VW disease could reflect a more active phase of disease (74).

† Plaque characterization has mainly been performed in the Asian population, in which large multicomponent atherosclerotic plaques are significantly more prevalent. Several case series have shown the possibility of detecting intraplaque hemorrhage (22,89–93); however, postmortem studies suggest that intraplaque hemorrhage has a lower prevalence in intracranial plaques compared with extracranial (carotid) plaques (6,47,94); therefore, its role so far remains elusive.

atherosclerosis with or without arterial remodeling, and less frequently Moyamoya vasculopathy, dissections, and cerebral aneurysms (all mostly for research purposes). When 3-T VW imaging does not show any abnormalities, when the clinician suspects subtle VW disease, or when all arteries of the circle of Willis need to be thoroughly assessed and/or screened, our 7-T protocol can be considered if this platform is available.

Systematic Approach of VW Assessment

General Assessment

VW imaging assessment at our institution is generally performed on specialized workstations for diagnostic imaging with a high-resolution monitor and a picture archiving and communication system (IDS7; Sectra AB, Linköping, Sweden). When an intracranial arterial stenosis has been found at TOF MR angiography, VW imaging could entail a dedicated characterization of this lesion on VW images (8). In practice, this is a less common situation in our patient population, so we perform a complete search of the large intracranial vasculature, starting at the extracranial internal carotid and vertebral artery and then following the course of these arteries into the basilar artery and anterior, middle, and posterior cerebral artery branches, including the M1, (very) proximal M2, A1, (very) proximal A2, P1, and (very) proximal P2 segments. For all currently published VW imaging sequences, including our own sequences, voxel size exceeds the VW thickness of all arteries and will result in overestimation of wall thickness. Lesions are visible, though, as they generally have a higher intensity or thicker appearance than the adjacent, apparently normal VW. In our experience, most intracranial VW lesions are detectable when scrutinizing the source data of the VW imaging sequences, that is, when the images are acquired in a transverse (7 T) or transverse oblique plane (3 T) (43). However, multiplanar reformatting–when applicable–may increase diagnostic confidence of some lesions, including lesions of the M1 segment of the MCA, which is one of the few circle of Willis vessels visualized solely parallel to its orientation in a transverse section (Fig 1).

Before using intracranial VW imaging as a diagnostic tool in patients, one should become acquainted with the normal appearance of the arterial wall on VW images (Figs 1, 3). The normal VW can be seen as a thin line surrounding the vessel lumen and is isointense to the brain parenchyma (white and gray matter have approximately the same signal intensity on VW images because sequence parameters are specifically optimized for the VW). VW imaging of healthy intracranial vasculature frequently suggests a variance in wall thickness that is most likely not related to VW disease but due to partial volume effects. With normal ageing, the VW has been shown to increase in thickness; however, the question remains whether this small increase in
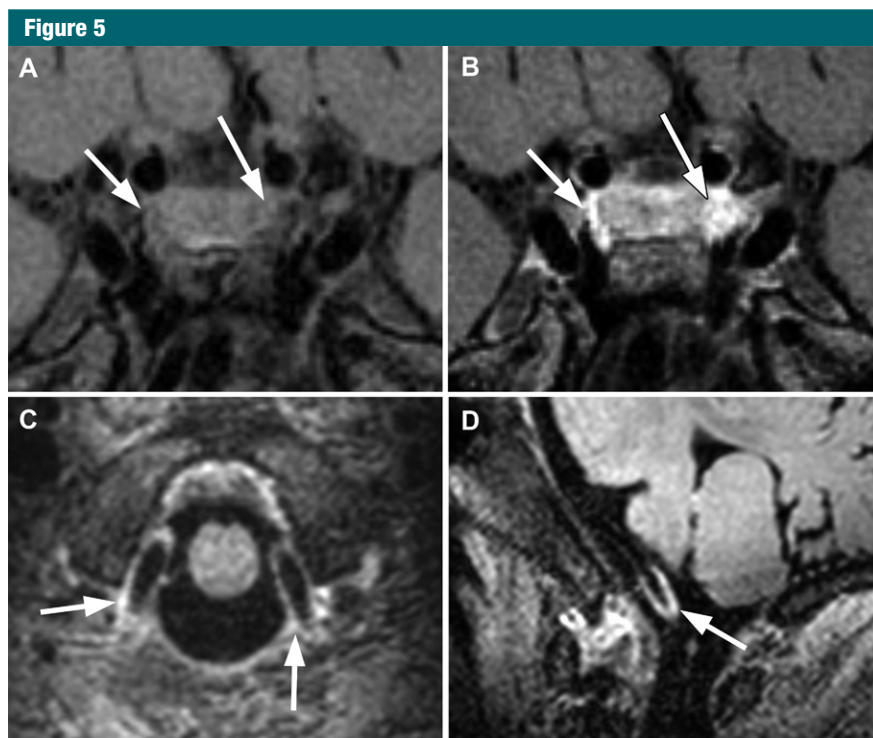
Figure 5

Figure 5: *A, B,* 3-T pre- *(A)* and postcontrast *(B)* T1-weighted VW images (voxel size, 0.5 × 0.5 × 1.0 mm³) in a 40-year-old woman with a recent right-sided ischemic stroke, zoomed in on the cavernous sinus. The postcontrast image of the cavernous sinus shows diffuse contrast enhancement of the cavernous plexus (arrows), which makes delineation of the carotid VW challenging. *C, D,* 7-T postcontrast T1-weighted magnetization-prepared inversion-recovery TSE images in the same subject, zoomed in on the vertebral arteries that cross the dura mater. In transverse orientation *(C),* contrast enhancement (arrows) of both vertebral arteries can be seen when crossing the dura mater. In sagittal orientation *(D),* this enhancement can be better appreciated (arrow) at the same location of the transdural crossing of the vertebral arteries.

thickness can be visualized with the currently used spatial resolutions (45). In younger patients without significant brain atrophy, the MCA is often located directly adjacent to the brain parenchyma, with little or no visible CSF in between. Because its signal intensity is similar to that of brain parenchyma in most sequences, it is often difficult to assess all segments of the MCA VW (including possible lesions) (Fig 3).

In general, a VW lesion is defined by one or both of the following characteristics (Fig 4): *(a)* a focal or more diffuse thickening of the VW greater than 50% compared with the adjacent VW thickness (31) and/or *(b)* focal or diffuse vivid contrast enhancement (56). One can further characterize the lesion as eccentric–less than 50% of the circumference of the VW–or concentric–greater than 50% of

the circumference–and as enhancing or not enhancing after contrast agent administration (see below), which can give an indication of the specific underlying disease process (Table 3). When assessing a potential lesion, the area of interest should be compared with next sections (in case of concentric thickening) or the cross-section of the VW should be scrutinized (in case of eccentric thickening), and it should be compared with the contralateral VW (but beware of bilateral disease). Finally, VW images should be cross-correlated with the axial TOF MR angiographic images for correct interpretation of the specific artery/arteries in which the lesion(s) was/were found and to check if the lesion causes luminal narrowing. Bear in mind that due to arterial remodeling, VW lesions very often do not show a stenosis (15); therefore, the

absence of stenosis should not be an argument in the decision process whether a lesion is present or not.

Contrast Enhancement

Ideally, both pre- and postcontrast images are available for assessment of VW lesion enhancement. With this setup, contrast-enhancing lesions can be distinguished more accurately from nonenhancing lesions with a high signal intensity. To this end, we either compare pre- and postcontrast images one-on-one (eyeballing) or we calculate subtraction images (postcontrast minus precontrast), for example, using MeVisLab (version 2.5; MeVis Medical Solutions, Bremen, Germany). However, as mentioned before, time constraints often limit VW imaging in clinical practice to one postcontrast VW imaging sequence. When only postcontrast images are available, assessment of contrast enhancement will be based on a comparison of the relative signal intensity of the arterial VW (lesion) with the appearance of the other (contralateral) arterial VW, the signal of the brain tissue, and/or the pituitary stalk. The pituitary stalk shows vivid contrast enhancement (57), and when the signal intensity of an intracranial arterial VW lesion approximates that of the pituitary stalk, it can be considered as contrast enhancement (Fig 4). Contrarily, if the signal intensity follows the intensity of the brain parenchyma, this can be considered as absence of enhancement.

In healthy subjects, contrast enhancement of the internal carotid artery and vertebral artery wall can be seen at the location where these arteries cross the dura mater and should not be mistaken for pathologic contrast enhancement (Fig 5). Vasa vasorum and increased permeability of the endothelium have been described at this location, but the exact nature of this contrast enhancement has yet to be determined (58). Also, the cavernous sinus shows diffuse enhancement after contrast agent administration; since the internal carotid artery runs through this cavernous venous plexus, it is difficult to assess the presence or absence of contrast enhancement of
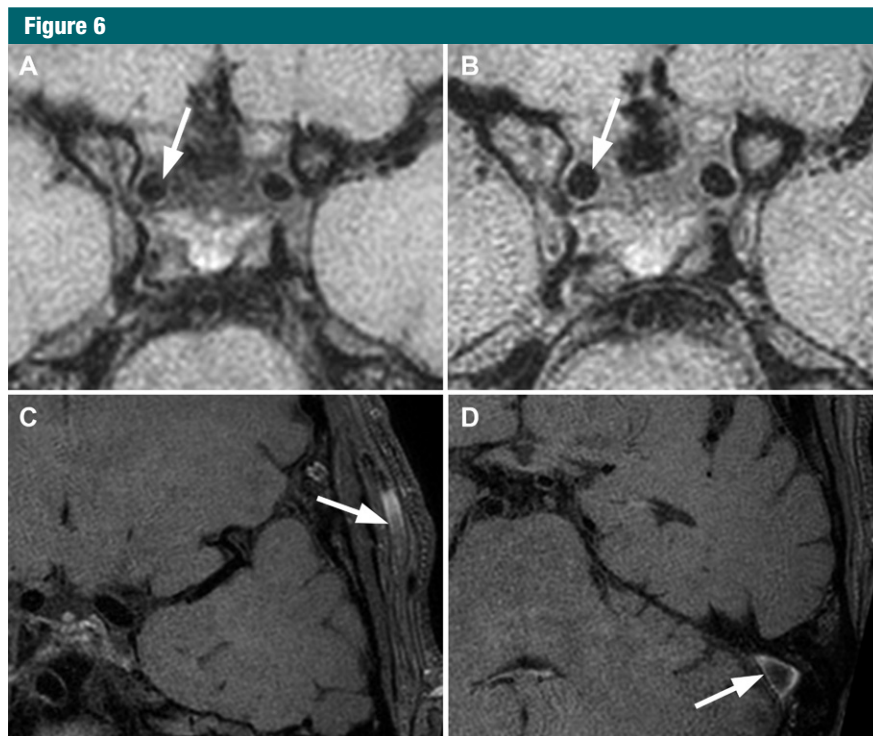
Figure 6: *A, B,* 3-T precontrast T1–weighted VW images (voxel size, 0.5 × 0.5 × 1.0 mm³) in a 38-year-old healthy man. *A,* An isointense artifact is seen in the lumen of the right ICA (arrow). *B,* A repeated VW sequence in the same imaging session did not show the isointense artifact in the lumen (arrow). *C, D,* 3-T transverse oblique postcontrast T1-weighted VW images in a 58-year-old healthy man. Hyperintense venous slow-flow artifacts are seen in the extracranial veins (arrow in *C*). Hyperintensity caused by slow flow is present in the complete vein, but is more prominent along the VWs. Slow-flow–related hyperintensity can also be observed in the left sigmoid sinus (arrow in *D*).

Figure 7: An example of a free induction decay artifact on a 3-T precontrast T1-weighted VW image (voxel size, 0.5 × 0.5 × 1.0 mm³). A dashed pattern is seen over the left hemisphere (white arrowheads). When the artifact is present at the same location of a VW (black arrowhead) it hampers interpretation of VW abnormalities.

this cavernous segment of the internal carotid artery (Fig 5).

Common Artifacts and Corresponding Pitfalls

Like all MR imaging examinations, VW imaging is sensitive to motion artifacts, even more so because of the relatively long acquisition times. Also, sensitivity encoding fold-over artifacts need to be considered when deciding to use a VW imaging sequence with sensitivity encoding acceleration. Next to these more general artifacts, there are two artifacts that may pose an interpretation problem specifically when assessing VW images. The first is the slow-flow artifact (Fig 6). Due to the parabolic flow velocity profile within a vessel, the flow directly next to the VW is slower compared with the center of the lumen. Intracranial VW imaging sequences that use the inflow or outflow of blood to suppress the arterial lumen can therefore show a higher signal from unsuppressed blood near the VW, which mimics either the VW itself (making it appear thickened) or mimics a focal VW lesion (when flow is focally decreased). These hyperintense artifacts can be present both before and after contrast agent administration but are in principle more visible after contrast agent injection (Fig 6).

Slow-flow artifacts are most obvious in the slow-flowing blood in smaller and larger veins, for instance in veins within the Sylvian cistern that are in relatively close proximity to the branches of the MCA. When solely interpreting VW images, slow flow in veins can be misinterpreted as arterial wall enhancement. This misinterpretation can be avoided by routinely cross-checking the location of the intracranial arteries on TOF MR angiographic images or by assessing the pattern of the hyperintense signal: Slow-flow artifacts are often symmetrically present in both hemispheres and can be seen in many vascular structures both inside the skull and in the extracranial veins, such as the superficial temporal vein (Fig 6). Suboptimal suppression of slow flow is related to the VW imaging technique used, and although TOF MR angiography is also
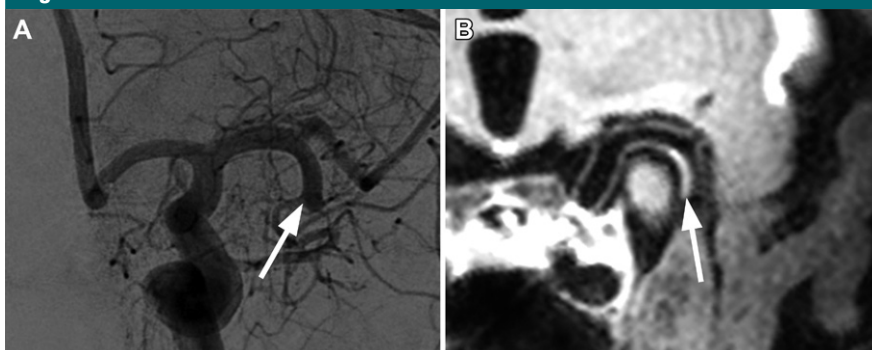
Figure 8

Figure 8: Images in a 85-year-old man with a recent occlusion of the left MCA, successfully treated with mechanical thrombectomy. *A,* Intra-arterial digital subtraction angiogram obtained directly before the mechanical thrombectomy procedure shows an acute cut-off in the MCA (arrow). *B,* 7-T T1-weighted magnetization-prepared inversion-recovery TSE image shows clear VW enhancement in the MCA at the location of the M1-M2 segment (arrow), where the thrombectomy device removed the occluding thrombus.
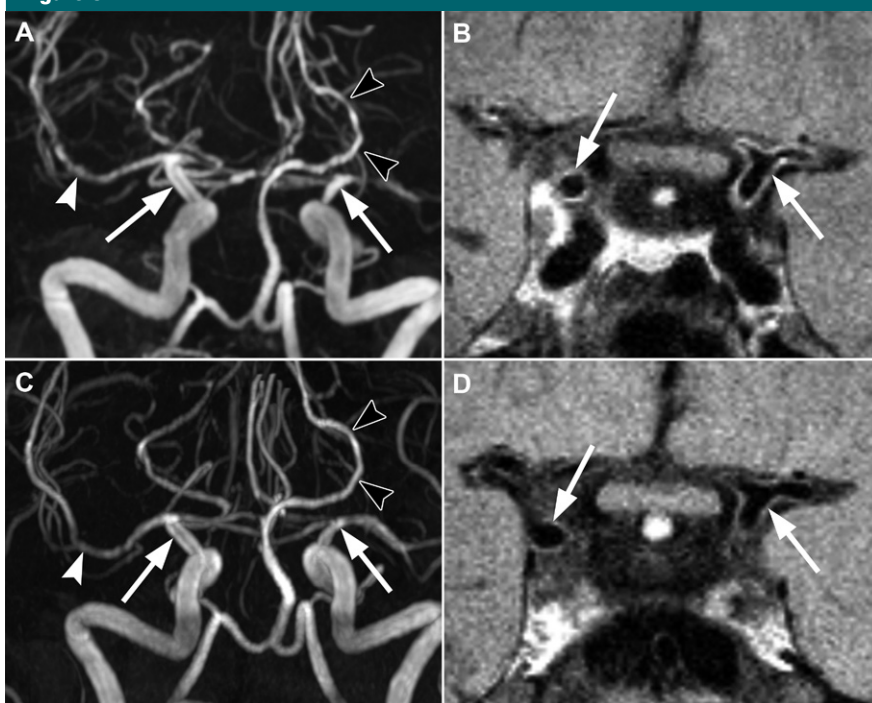
Figure 9

Figure 9: VW images in a 47-year-old man with a clinically proven primary angiitis of the central nervous system. Although biopsy findings were inconclusive, digital subtraction angiography showed extensive central and peripheral segmental arterial narrowing. *A, C,* 3-T coronal maximum intensity projections of 3D TOF MR angiography and, *B, D,* 3-T transverse postcontrast T1-weighted VW images (voxel size, 0.5 × 0.5 × 1.0 mm³) at presentation *(A, B)* and 7 months after immunosuppressive therapy *(C, D).* At presentation, TOF MR angiogram shows multisegmental luminal narrowing in the PCA and MCA (respective black and white arrowheads on, *A*) and left distal ICA (right arrow), while the corresponding VW images (voxel size, 0.5 × 0.5 × 1.0 mm³) *(B, D)* show more extensive disease, with clear concentric VW enhancement of the left distal ICA A1-M1 bifurcation (right arrow), as well as the right distal ICA (left arrow). After therapy, a reduction in the multisegmental luminal narrowing can be seen on the TOF MR angiogram (respective black and white arrowheads on, *C*), while T1-weighted VW image shows resolution of VW enhancement in both distal ICAs (arrows).

prone to slow-flow artifacts, it rarely occurs that these artifacts occur at the exact same location at both sequences. When in doubt about whether a VW abnormality is a slow-flow artifact or a real VW lesion, we do not want to judge every abnormality as a VW lesion, but we analyse every possible lesion with caution; when in doubt, we may not call it a VW lesion; when the hyperintense signal is too large in volume for a thin arterial VW, we consider it a slow-flow artifact.

The other artifact that can cause difficulties in interpretation of VW abnormalities is the free-induction decay artifact (Fig 7). This artifact is caused by repeated refocusing radiofrequency pulses within the short echo times of T1-weigthed VW imaging sequences. The artifact occurs when the free-induction decays from the refocusing pulses are not completely spoiled and appears as a linear dashed pattern on the image (59). The VW will show the same dashed, "zigzag" pattern, making it difficult to differentiate between artifact and VW thickening and/or lesion. Possible ways to minimize this artifact is to increase the number of signals acquired, increase the echo time, or choose a larger section thickness; however, for obvious reasons these are difficult to implement in intracranial VW imaging.

VW Disease

Although intracranial VW imaging is still in its developmental stage, there are already several challenging diagnostic situations in which it has shown its potential value (1,2,60,61), the most important of which is determining the cause of stroke and assessing accompanying VW lesions. Recently, two excellent review papers have been published that both address the commonly found imaging characteristics of different types of intracranial VW disease, including a thorough literature overview (2,62). We will therefore restrict this section to a compact overview table (Table 3) for hands-on use in clinical practice, including illustrative image examples (Figs 4, 8–12).
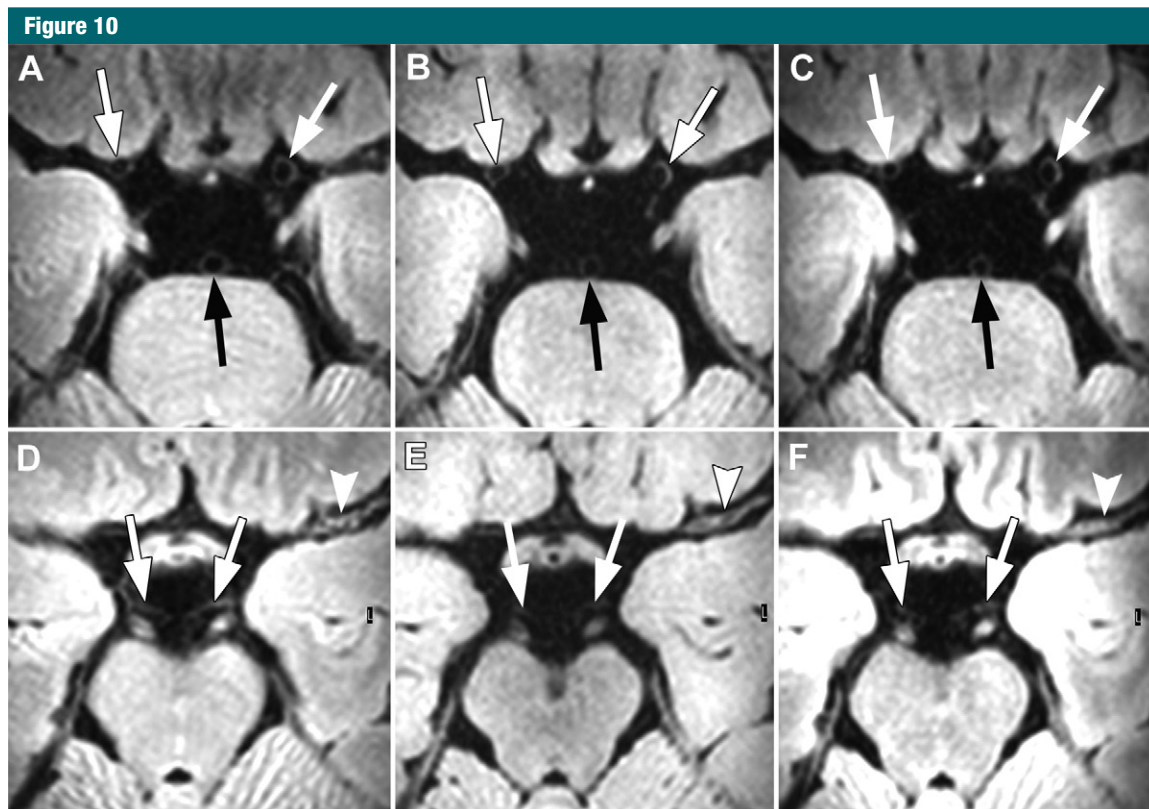
Figure 10:   7-T transverse T1-weighted magnetization-prepared inversion-recovery TSE *(A, D)*, whole-brain T1-weighted *(B, E)*, and T2-weighted magnetization-prepared inversion-recovery TSE images *(C, F)* in a 31-year-old man with Moyamoya disease. The VW of the left distal ICA (left white arrow in *A–C*) is slightly more hyperintense compared with the right distal ICA (right white arrow in *A–C*) and basilar artery (black arrow in *A–C*). Both distal ICAs are relatively narrow compared with the basilar artery. *D–F,* Left MCA is seen to be almost occluded with VW thickening (arrowhead). The VWs of the P1 segment of the PCA are also visible (arrows). (Reprinted, with permission, from reference 48.)

Future Prospects

Technical Developments

As discussed in the previous paragraphs, the difficulty in intracranial VW imaging is that ideally, one strives for a maximum spatial resolution to detect lesions of the small intracranial arterial VWs and maximum suppression of both blood signal within and CSF signal surrounding the arteries. Both will significantly increase acquisition time. For clinical implementation, acquisition time reduction is necessary to perform both pre- and postcontrast VW imaging within a clinical MR imaging time slot (approximately 25–35 minutes), without a substantial decrease in SNR and CNR of the arterial VW. Innovative methods for reducing acquisition time (eg, compressed sensing [63,64]), as well as different

CSF suppression techniques (DANTE [19,20,65], antidriven-equilibrium [32,33]), in combination with various 2D and 3D acquisition methods with different coverage, need to be compared in the upcoming years.

Spatial coverage.—At 3 T, most sequences are limited to a region that covers either the circle of Willis or the (known) stenotic VW lesion, with a few surrounding centimeters. An option for "increasing coverage" is to acquire the VW images in a more angulated coronal plane and include the proximal vertebral arteries, as we generally do with our 3-T sequence. "Real" whole-brain coverage–that is, increasing the FOV–benefits from nonselective pulses (shorter echo spacing in TSE trains), 2D sensitivity encoding, and no need for oversampling (48). However, because flow suppression is often based

on dephasing during the echo train, with too short echo train lengths flow suppression will inevitably decrease.

Next to improvements in pulse sequence design, hardware improvements may also show promise in VW imaging. Recently, an advanced coil system for joint intracranial and extracranial VW imaging has been developed (66). This coil system provides the opportunity to image both intracranial and extracranial arteries at once for an optimal assessment of the association of carotid and intracranial atherosclerotic plaques and ischemic stroke within a reasonable imaging time (5 minutes 54 seconds to 7 minutes 36 seconds).

Acquisition time.—Efficient k-space sampling trajectories (view-ordering) in combination with parallel imaging techniques have been described to

reduce acquisition time in 3D TSE sequences, while the trajectories can also be optimized for reduced T2 weighting (17,23). Compressed sensing allows image reconstruction from fewer k-space data and, thus, shorter imaging times. Compressed sensing needs yet to be investigated for intracranial VW imaging but might be a way to further reduce the acquisition time (63,64).

In current protocols, several imaging parameters can be varied to counterbalance the relatively long acquisition time, such as the oversample factor, TSE train length, and image acceleration by parallel imaging such as sensitivity encoding that leads to a change in imaging time (1,21,31,40). However, all of these techniques sacrifice spatial resolution and/or SNR in the process or need more advanced hardware (eg, a higher number of receiver coils or multiband imaging) to overcome the inevitable cost in image quality.

Clinical Considerations

Because no standard of reference in vivo method for intracranial arterial VW disease is available, histologic validation of intracranial VW imaging is essential. Since no tissue can be obtained while the patient is alive–compared with, for example, endarterectomy samples in carotid artery disease–validation can only be performed in postmortem studies. A series of postmortem validation studies has been performed at 7 T by using ex vivo circle of Willis specimens from patients with and without a history of cerebrovascular disease, as well as from patients with intracranial aneurysms (47,67–71). These studies found clear correlations between VW and atherosclerotic plaques detected on VW images and histopathologic findings, best seen on T1-weighted
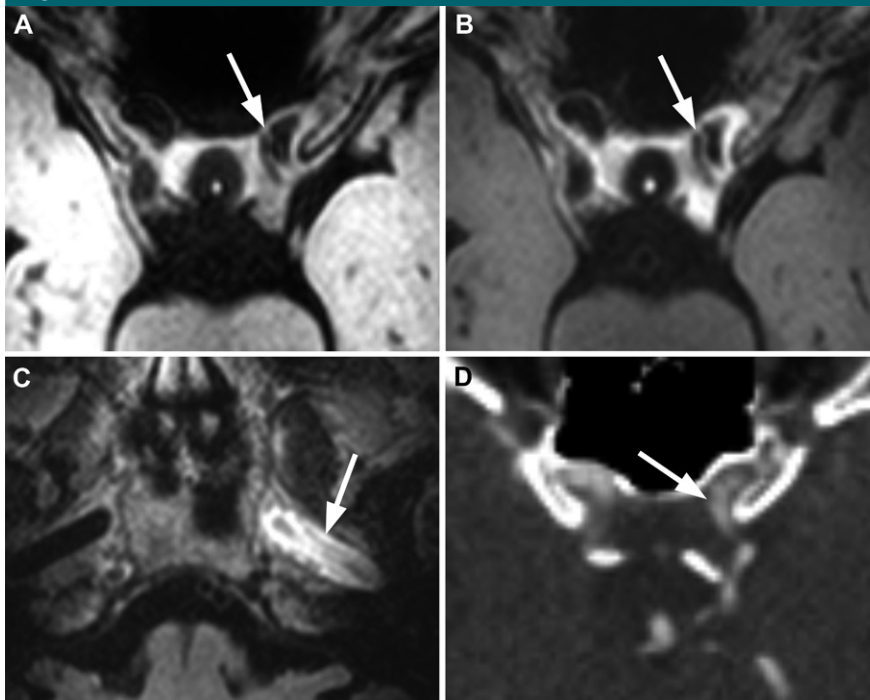

Figure 11: A–C, 7-T transverse VWI images in a 44-year-old woman with a spontaneous dissection of the left ICA, imaged 4 days after symptom onset. A, B, Precontrast (A) and postcontrast (B) T1-weighted magnetization-prepared inversion-recovery TSE images show a tapering of the lumen and VW enhancement (arrow) of the left distal ICA. C, Diffuse concentric VW enhancement and a dissection flap are seen on the postcontrast image more proximally in the left distal ICA at the skull base (arrow). D, Tapering of the distal ICA can also be appreciated on a CT angiogram, reformatted in the same orientation as, A, and, B.
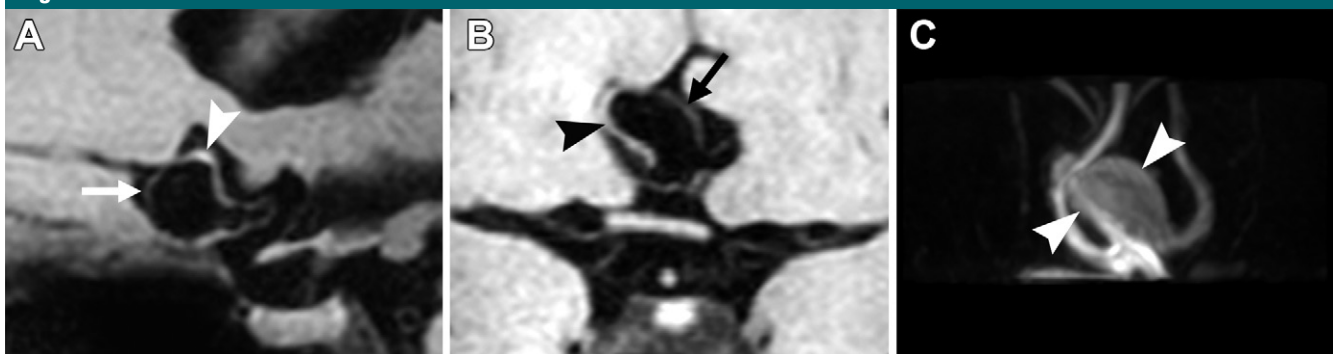

Figure 12: 7-T precontrast sagittal (A) and coronal (B) T1-weighted magnetization-prepared inversion-recovery TSE images of an anterior communicating artery aneurysm. The aneurysm wall shows a variation in wall thickness: The left lateral side and top of the aneurysm can be seen to have a thicker wall (white and black arrowheads), while the right lateral and anterior part of the aneurysm show a thinner wall (white and black arrows). C, 7-T maximum intensity projection of 3D TOF MR angiography shows the corresponding anatomic geometry of the aneurysm (arrowheads).

Radiology

sequences (47,67,68,70,71). However, more insight into what normal ageing of the VW looks like on VW images and what underlying mechanisms can cause VW (lesion) enhancement are still needed. This has proven to be a challenge, because methods to preserve tissue in ex vivo studies (eg, fixation and tissue temperature effects) change the MR imaging characteristics of the tissue so that results from these studies cannot be directly translated to in vivo VW imaging, while functional measures, such as lesion enhancement after contrast agent administration, cannot be performed in postmortem studies.

Conclusion

Intracranial VW imaging has become part of state-of-the-art MR imaging protocols detecting causes of ischemic stroke, mainly in a research setting but increasingly asked for (and used) in clinical practice. It has tentatively shown commonly seen VW changes in patients with diseases including, but not limited to, central nervous system vasculitis, Moyamoya disease, aneurysms, dissections, and intracranial atherosclerosis. However, its precise role and added value for prognosis and patient care needs further elucidation. A field strength of at least 3 T enables VW imaging sequences with high enough CNR and spatial resolution to assess the thin intracranial atherosclerotic VW and detect and ultimately characterize VW lesions. Radiologists should be aware of the normal appearance (variance) of the VW on intracranial VW images, the main characteristics of VW lesions that may help differentiate between different VW pathologic conditions, and the technical limitations and pitfalls in the assessment of intracranial VW imaging. Further technical improvements will enable (among others) reduced acquisition time, while further histologic validation of these VW imaging sequences will aid in a better understanding of normal VW thickness variance, ultimately leading to better knowledge of the underlying

pathologic conditions of lesions seen on VW images.

References

1. Dieleman N, van der Kolk AG, Zwanenburg JJ, et al. Imaging intracranial vessel wall pathology with magnetic resonance imaging: current prospects and future directions. Circulation 2014;130(2):192–201.

2. Mandell DM, Mossa-Basha M, Qiao Y, et al. Intracranial vessel wall MRI: principles and expert consensus recommendations of the American Society of Neuroradiology. AJNR Am J Neuroradiol 2017;38(2):218–229.

3. Gorelick PB, Wong KS, Bae HJ, Pandey DK. Large artery intracranial occlusive disease: a large worldwide burden but a relatively neglected frontier. Stroke 2008;39(8):2396–2399.

4. Arenillas JF. Intracranial atherosclerosis: current concepts. Stroke 2011;42(1 Suppl):S20–S23.

5. Qureshi AI, Caplan LR. Intracranial atherosclerosis. Lancet 2014;383(9921):984–998.

6. Ritz K, Denswil NP, Stam OC, van Lieshout JJ, Daemen MJ. Cause and mechanisms of intracranial atherosclerosis. Circulation 2014;130(16):1407–1414.

7. Chimowitz MI, Lynn MJ, Howlett-Smith H, et al. Comparison of warfarin and aspirin for symptomatic intracranial arterial stenosis. N Engl J Med 2005;352(13):1305–1316.

8. Holmstedt CA, Turan TN, Chimowitz MI. Atherosclerotic intracranial arterial stenosis: risk factors, diagnosis, and treatment. Lancet Neurol 2013;12(11):1106–1114.

9. Derdeyn CP, Chimowitz MI, Lynn MJ, et al. Aggressive medical treatment with or without stenting in high-risk patients with intracranial artery stenosis (SAMMPRIS): the final results of a randomised trial. Lancet 2014;383(9914):333–341.

10. Bos D, Portegies ML, van der Lugt A, et al. Intracranial carotid artery atherosclerosis and the risk of stroke in whites: the Rotterdam Study. JAMA Neurol 2014;71(4):405–411.

11. Bos D, van der Rijk MJ, Geeraedts TE, et al. Intracranial carotid artery atherosclerosis: prevalence and risk factors in the general population. Stroke 2012;43(7):1878–1884.

12. Homburg PJ, Plas GJ, Rozie S, van der Lugt A, Dippel DW. Prevalence and calcification of intracranial arterial stenotic lesions as assessed with multidetector computed tomography angiography. Stroke 2011;42(5):1244–1250.

13. Vos A, Van Hecke W, Spliet WG, et al. Predominance of nonatherosclerotic internal elastic lamina calcification in the intracranial internal carotid artery. Stroke 2016;47(1):221–223.

14. Nguyen-Huynh MN, Wintermark M, English J, et al. How accurate is CT angiography in evaluating intracranial atherosclerotic disease? Stroke 2008;39(4):1184–1188.

15. van der Kolk AG, Zwanenburg JJ, Brundel M, et al. Intracranial vessel wall imaging at 7.0-T MRI. Stroke 2011;42(9):2478–2484.

16. van der Kolk AG, Hendrikse J, Zwanenburg JJ, Visser F, Luijten PR. Clinical applications of 7 T MRI in the brain. Eur J Radiol 2013;82(5):708–718.

17. Qiao Y, Steinman DA, Qin Q, et al. Intracranial arterial wall imaging using three-dimensional high isotropic resolution black blood MRI at 3.0 Tesla. J Magn Reson Imaging 2011;34(1):22–30.

18. Zhu C, Haraldsson H, Tian B, et al. High resolution imaging of the intracranial vessel wall at 3 and 7 T using 3D fast spin echo MRI. MAGMA 2016;29(3):559–570.

19. Xie Y, Yang Q, Xie G, Pang J, Fan Z, Li D. Improved black-blood imaging using DANTE-SPACE for simultaneous carotid and intracranial vessel wall evaluation. Magn Reson Med 2016;75(6):2286–2294.

20. Wang J, Helle M, Zhou Z, Börnert P, Hatsukami TS, Yuan C. Joint blood and cerebrospinal fluid suppression for intracranial vessel wall MRI. Magn Reson Med 2016;75(2):831–838.

21. Zhang L, Zhang N, Wu J, et al. High resolution three dimensional intracranial arterial wall imaging at 3 T using T1 weighted SPACE. Magn Reson Imaging 2015;33(9):1026–1034.

22. Li ML, Xu YY, Hou B, et al. High-resolution intracranial vessel wall imaging using 3D CUBE T1 weighted sequence. Eur J Radiol 2016;85(4):803–807.

23. Busse RF, Brau AC, Vu A, et al. Effects of refocusing flip angle modulation and view ordering in 3D fast spin echo. Magn Reson Med 2008;60(3):640–649.

24. Weigel M, Hennig J. Diffusion sensitivity of turbo spin echo sequences. Magn Reson Med 2012;67(6):1528–1537.

25. Edelman RR, Chien D, Kim D. Fast selective black blood MR imaging. Radiology 1991;181(3):655–660.

26. Wang J, Yarnykh VL, Yuan C. Enhanced image quality in black-blood MRI using the improved motion-sensitized driven-equilibrium (iMSDE) sequence. J Magn Reson Imaging 2010;31(5):1256–1263.

27. Ma N, Jiang WJ, Lou X, et al. Arterial remodeling of advanced basilar atherosclerosis: a 3-tesla MRI study. Neurology 2010;75(3):253–258.

28. Zhu XJ, Du B, Lou X, et al. Morphologic characteristics of atherosclerotic middle cerebral arteries on 3T high-resolution MRI. AJNR Am J Neuroradiol 2013;34(9):1717–1722.

29. Gutierrez J, Goldman J, Honig LS, Elkind MS, Morgello S, Marshall RS. Determinants of cerebrovascular remodeling: do large brain arteries accommodate stenosis? Atherosclerosis 2014;235(2):371–379.

30. Qiao Y, Anwar Z, Intrapiromkul J, et al. Patterns and implications of intracranial arterial remodeling in stroke patients. Stroke 2016;47(2):434–440.

31. Swartz RH, Bhuta SS, Farb RI, et al. Intracranial arterial wall imaging using high-resolution 3-tesla contrast-enhanced MRI. Neurology 2009;72(7):627–634.

32. Fan Z, Yang Q, Deng Z, et al. Whole-brain intracranial vessel wall imaging at 3 Tesla using cerebrospinal fluid-attenuated T1-weighted 3D turbo spin echo. Magn Reson Med 2017;77(3):1142–1150.

33. Yang H, Zhang X, Qin Q, Liu L, Wasserman BA, Qiao Y. Improved cerebrospinal fluid suppression for intracranial vessel wall MRI. J Magn Reson Imaging 2016;44(3):665–672.

34. Gutierrez J, Elkind MS, Petito C, Chung DY, Dwork AJ, Marshall RS. The contribution of HIV infection to intracranial arterial remodeling: a pilot study. Neuropathology 2013;33(3):256–263.

35. Qiao Y, Guallar E, Suri FK, et al. MR imaging measures of intracranial atherosclerosis in a population-based study. Radiology 2016;280(3):860–868.

36. Dobrin PB. Effect of histologic preparation on the cross-sectional area of arterial rings. J Surg Res 1996;61(2):413–415.

37. Tran T, Sundaram CP, Bahler CD, et al. Correcting the shrinkage effects of formalin fixation and tissue processing for renal tumors: toward standardization of pathological reporting of tumor size. J Cancer 2015;6(8):759–766.

38. Bouvy WH, Biessels GJ, Kuijf HJ, Kappelle LJ, Luijten PR, Zwanenburg JJ. Visualization of perivascular spaces and perforating arteries with 7 T magnetic resonance imaging. Invest Radiol 2014;49(5):307–313.

39. Lindenholz A, Harteveld AA, Siero JC, Zwanenburg JJ, Hendrikse J. A multiple comparison between 3T intracranial vessel wall sequences [abstr]. In: Proceedings of the Twenty-Fourth Meeting of the International Society for Magnetic Resonance in Medicine. Berkeley, Calif: International Society for Magnetic Resonance in Medicine, 2016; 1065.

40. Ryu CW, Jahng GH, Kim EJ, Choi WS, Yang DM. High resolution wall and lumen MRI of the middle cerebral arteries at 3 tesla. Cerebrovasc Dis 2009;27(5):433–442.

41. Lee WJ, Choi HS, Jang J, et al. Non-stenotic intracranial arteries have atherosclerotic changes in acute ischemic stroke patients: a 3T MRI study. Neuroradiology 2015;57(10):1007–1013.

42. Dieleman N, Yang W, Abrigo JM, et al. Magnetic resonance imaging of plaque morphology, burden, and distribution in patients with symptomatic middle cerebral artery stenosis. Stroke 2016;47(7):1797–1802.

43. Dieleman N, Yang W, van der Kolk AG, et al. Qualitative evaluation of a high-resolution 3D multi-sequence intracranial vessel wall protocol at 3 tesla MRI. PLoS One 2016;11(8):e0160781.

44. Xu WH, Li ML, Gao S, et al. In vivo high-resolution MR imaging of symptomatic and asymptomatic middle cerebral artery atherosclerotic stenosis. Atherosclerosis 2010;212(2):507–511.

45. Harteveld AA, van der Kolk AG, van der Worp HB, et al. High-resolution intracranial vessel wall MRI in an elderly asymptomatic population: comparison of 3T and 7T. Eur Radiol 2017;27(4):1585–1595.

46. Oppenheim C, Naggara O, Touzé E, et al. High-resolution MR imaging of the cervical arterial wall: what the radiologist needs to know. RadioGraphics 2009;29(5):1413–1431.

47. Harteveld AA, Denswil NP, Siero JC, et al. Quantitative intracranial atherosclerotic plaque characterization at 7T MRI: an ex vivo study with histologic validation. AJNR Am J Neuroradiol 2016;37(5):802–810.

48. van der Kolk AG, Hendrikse J, Brundel M, et al. Multi-sequence whole-brain intracranial vessel wall imaging at 7.0 tesla. Eur Radiol 2013;23(11):2996–3004.

49. Teeuwisse WM, Brink WM, Webb AG. Quantitative assessment of the effects of high-permittivity pads in 7 Tesla MRI of the brain. Magn Reson Med 2012;67(5):1285–1293.

50. Ellingson BM, Bendszus M, Boxerman J, et al. Consensus recommendations for a standardized brain tumor imaging protocol in clinical trials. Neuro Oncol 2015;17(9):1188–1198.

51. Fayad ZA. MR imaging for the noninvasive assessment of atherothrombotic plaques. Magn Reson Imaging Clin N Am 2003;11(1):101–113.

52. Harteveld AA, De Cocker LJ, Dieleman N, et al. High-resolution postcontrast time-of-flight MR angiography of intracranial perforators at 7.0 Tesla. PLoS One 2015;10(3):e0121051.

53. van der Kolk AG, Zwanenburg JJ, Brundel M, et al. Distribution and natural course of intracranial vessel wall lesions in patients with ischemic stroke or TIA at 7.0 Tesla MRI. Eur Radiol 2015;25(6):1692–1700.

54. Seo WK, Oh K, Suh SI, Seol HY. Clinical significance of wall changes after recanalization therapy in acute stroke: high-resolution vessel wall imaging. Stroke 2017;48(4):1077–1080.

55. Power S, Matouk C, Casaubon LK, et al. Vessel wall magnetic resonance imaging in acute ischemic stroke: effects of embolism and mechanical thrombectomy on the arterial wall. Stroke 2014;45(8):2330–2334.

56. Qiao Y, Zeiler SR, Mirbagheri S, et al. Intracranial plaque enhancement in patients with cerebrovascular events on high-spatial-resolution MR images. Radiology 2014;271(2):534–542.

57. de Rotte AA, van der Kolk AG, Rutgers D, et al. Feasibility of high-resolution pituitary MRI at 7.0 tesla. Eur Radiol 2014;24(8):2005–2011.

58. Portanova A, Hakakian N, Mikulis DJ, Virmani R, Abdalla WM, Wasserman BA. Intracranial vasa vasorum: insights and implications for imaging. Radiology 2013;267(3):667–679.

59. Morelli JN, Runge VM, Ai F, et al. An image-based approach to understanding the physics of MR artifacts. RadioGraphics 2011;31(3):849–866.

60. Kontzialis M, Wasserman BA. Intracranial vessel wall imaging: current applications

and clinical implications. Neurovasc Imaging 2016;2:4.

61. de Havenon A, Chung L, Park M, Mossa-Basha M. Intracranial vessel wall MRI: a review of current indications and future applications. Neurovasc Imaging 2016;2:10.

62. Bhogal P, Navaei E, Makalanda HL, et al. Intracranial vessel wall MRI. Clin Radiol 2016;71(3):293–303.

63. Lustig M, Donoho D, Pauly JM. Sparse MRI: The application of compressed sensing for rapid MR imaging. Magn Reson Med 2007;58(6):1182–1195.

64. Li B, Li H, Li J, et al. Relaxation enhanced compressed sensing three-dimensional black-blood vessel wall MR imaging: preliminary studies. Magn Reson Imaging 2015;33(7):932–938.

65. Li L, Miller KL, Jezzard P. DANTE-prepared pulse trains: a novel approach to motion-sensitized and motion-suppressed quantitative magnetic resonance imaging. Magn Reson Med 2012;68(5):1423–1438.

66. Hu X, Li Y, Zhang L, Zhang X, Liu X, Chung YC. A 32-channel coil system for MR vessel wall imaging of intracranial and extracranial arteries at 3T. Magn Reson Imaging 2017;36:86–92.

67. Majidi S, Sein J, Watanabe M, et al. Intracranial-derived atherosclerosis assessment: an in vitro comparison between virtual histology by intravascular ultrasonography, 7T MRI, and histopathologic findings. AJNR Am J Neuroradiol 2013;34(12):2259–2264.

68. Turan TN, Rumboldt Z, Granholm AC, et al. Intracranial atherosclerosis: correlation between in-vivo 3T high resolution MRI and pathology. Atherosclerosis 2014;237(2):460–463.

69. Kleinloog R, Korkmaz E, Zwanenburg JJ, et al. Visualization of the aneurysm wall: a 7.0-tesla magnetic resonance imaging study. Neurosurgery 2014;75(6):614–622; discussion 622.

70. van der Kolk AG, Zwanenburg JJ, Denswil NP, et al. Imaging the intracranial atherosclerotic vessel wall using 7T MRI: initial comparison with histopathology. AJNR Am J Neuroradiol 2015;36(4):694–701.

71. Jiang Y, Zhu C, Peng W, et al. Ex-vivo imaging and plaque type classification of intracranial atherosclerotic plaque using high resolution MRI. Atherosclerosis 2016;249:10–16.

72. Li ML, Xu WH, Song L, et al. Atherosclerosis of middle cerebral artery: evaluation with high-resolution MR imaging at 3T. Atherosclerosis 2009;204(2):447–452.

73. Mandell DM, Matouk CC, Farb RI, et al. Vessel wall MRI to differentiate between reversible cerebral vasoconstriction syndrome and central nervous system vasculitis: preliminary results. Stroke 2012;43(3):860–862.

74. Obusez EC, Hui F, Hajj-Ali RA, et al. High-resolution MRI vessel wall imaging: spatial and temporal patterns of reversible cerebral vasoconstriction syndrome and central nervous system vasculitis. AJNR Am J Neuroradiol 2014;35(8):1527–1532.

75. Kim JM, Jung KH, Sohn CH, et al. High-resolution MR technique can distinguish moyamoya disease from atherosclerotic occlusion. Neurology 2013;80(8):775–776.

76. Mossa-Basha M, de Havenon A, Becker KJ, et al. Added value of Vessel wall magnetic resonance imaging in the differentiation of Moyamoya vasculopathies in a non-Asian cohort. Stroke 2016;47(7):1782–1788.

77. Ryoo S, Cha J, Kim SJ, et al. High-resolution magnetic resonance wall imaging findings of Moyamoya disease. Stroke 2014;45(8):2457–2460.

78. Aoki S, Hayashi N, Abe O, et al. Radiation-induced arteritis: thickened wall with prominent enhancement on cranial MR images report of five cases and comparison with 18 cases of Moyamoya disease. Radiology 2002;223(3):683–688.

79. Yu LB, Zhang Q, Shi ZY, Wang MQ, Zhang D. High-resolution Magnetic Resonance Imaging of Moyamoya Disease. Chin Med J (Engl) 2015;128(23):3231–3237.

80. Arai D, Satow T, Komuro T, Kobayashi A, Nagata H, Miyamoto S. Evaluation of the arterial wall in vertebrobasilar artery dissection using high-resolution magnetic resonance vessel wall imaging. J Stroke Cerebrovasc Dis 2016;25(6):1444–1450.

81. Wang Y, Lou X, Li Y, et al. Imaging investigation of intracranial arterial dissecting aneurysms by using 3 T high-resolution MRI and DSA: from the interventional neuroradiologists' view. Acta Neurochir (Wien) 2014;156(3):515–525.

82. Bachmann R, Nassenstein I, Kooijman H, et al. High-resolution magnetic resonance imaging (MRI) at 3.0 Tesla in the short-term follow-up of patients with proven cervical artery dissection. Invest Radiol 2007;42(6):460–466.

83. Fiebach J, Brandt T, Knauth M, Jansen O. MRI with fat suppression in the visualization of wall hematoma in spontaneous dissection of the internal carotid artery [in German]. Rofo 1999;171(4):290–293.

84. Nagahata S, Nagahata M, Obara M, et al. Wall enhancement of the intracranial aneurysms revealed by magnetic resonance vessel wall imaging using three-dimensional turbo spin-echo sequence with motion-sensitized driven-equilibrium: a sign of ruptured aneurysm? Clin Neuroradiol 2016;26(3):277–283.

85. Edjlali M, Gentric JC, Régent-Rodriguez C, et al. Does aneurysmal wall enhancement on vessel wall MRI help to distinguish stable from unstable intracranial aneurysms? Stroke 2014;45(12):3704–3706.

86. Matouk CC, Mandell DM, Günel M, et al. Vessel wall magnetic resonance imaging identifies the site of rupture in patients with multiple intracranial aneurysms: proof of principle. Neurosurgery 2013;72(3):492–496; discussion 496.

87. Kondo R, Yamaki T, Mouri W, et al. Magnetic resonance vessel wall imaging reveals rupture site in subarachnoid hemorrhage with multiple cerebral aneurysms [in Japanese]. No Shinkei Geka 2014;42(12):1147–1150.

88. Ducros A. Reversible cerebral vasoconstriction syndrome. Lancet Neurol 2012;11(10):906–917.

89. Wang J, Guan M, Yamada K, et al. In vivo validation of simultaneous non-contrast angiography and intraplaque hemorrhage (SNAP) magnetic resonance angiography: an intracranial artery study. PLoS One 2016;11(2):e0149130.

90. Park JK, Kim SH, Kim BS, Choi G, Jeong SY, Choi JC. Imaging of intracranial plaques with black-blood double inversion recovery MR imaging and CT. J Neuroimaging 2011;21(2):e64–e68.

91. Chen XY, Wong KS, Lam WW, Ng HK. High signal on T1 sequence of magnetic resonance imaging confirmed to be intraplaque haemorrhage by histology in middle cerebral artery. Int J Stroke 2014;9(4):E19.

92. Xu WH, Li ML, Gao S, et al. Middle cerebral artery intraplaque hemorrhage: prevalence and clinical relevance. Ann Neurol 2012;71(2):195–198.

93. Turan TN, Bonilha L, Morgan PS, Adams RJ, Chimowitz MI. Intraplaque hemorrhage in symptomatic intracranial atherosclerotic disease. J Neuroimaging 2011;21(2):e159–e161.

94. Chen XY, Wong KS, Lam WW, Zhao HL, Ng HK. Middle cerebral artery atherosclerosis: histological comparison between plaques associated with and not associated with infarct in a postmortem study. Cerebrovasc Dis 2008;25(1-2):74–80.